A single nucleotide substitution in *TaHKT1;5-D* controls shoot Na^+ accumulation in bread wheat

Chana Borjigin[1,2], Rhiannon K. Schilling[1,2,], Jayakumar Bose[2,3], Maria Hrmova[1,2,4], Jiaen Qiu[2,3], Stefanie Wege[2,3], Apriadi Situmorang[2], Chris Brien[2,5], Bettina Berger[2,5], Matthew Gilliham[2,3], Allison S. Pearson[1,2,3], Stuart J. Roy[1,2,6]

[1]Australian Centre for Plant Functional Genomics, The University of Adelaide, PMB 1, Glen Osmond, South Australia 5064, Australia; [2]School of Agriculture, Food and Wine, The University of Adelaide, PMB 1, Glen Osmond, South Australia 5064, Australia; [3]ARC Centre of Excellence in Plant Energy Biology, The University of Adelaide, PMB 1, Glen Osmond, South Australia 5064, Australia; [4]School of Life Sciences, Huaiyin Normal University, Huai'an 223300, China; [5]Australian Plant Phenomics Facility, The Plant Accelerator, The University of Adelaide, PMB 1, Glen Osmond, South Australia 5064, Australia; [6]ARC Industrial Transformation Research Hub for Wheat in a Hot Dry Climate, The University of Adelaide, PMB 1, Glen Osmond, South Australia 5064, Australia.

Rhiannon K. Schilling, School of Agriculture, Food and Wine, The University of Adelaide, PMB 1, Glen Osmond, South Australia 5064, Australia. E-mail: rhiannon.schilling@adelaide.edu.au

Funding

This project was funded by the Grains Research and Development Corporation (GRDC): Project UA00145, UA00151, and the GRDC and the International Wheat Yield Partnership (IWYP): Projects IWYP39/ACP0009; IWYP60/ANU00027. The Australian Centre for Plant

Functional Genomics (ACPFG) was jointly funded by the Australian Research Council (ARC) and the GRDC, SW was supported by the ARC DE160100804. The Plant Accelerator®, Australian Plant Phenomics Facility, is funded under the National Collaborative Research Infrastructure Strategy (NCRIS).

Abstract

Improving salinity tolerance in the most widely cultivated cereal, bread wheat (*Triticum aestivum* L.), is essential to increase grain yields on saline agricultural lands. A Portuguese landrace, Mocho de Espiga Branca accumulates up to 6 folds greater leaf and sheath sodium (Na^+) than two Australian cultivars, Gladius and Scout, under salt stress. Despite high leaf and sheath Na^+ concentrations, Mocho de Espiga Branca maintained similar salinity tolerance compared to Gladius and Scout. A naturally occurring single nucleotide substitution was identified in the gene encoding a major Na^+ transporter TaHKT1;5-D in Mocho de Espiga Branca, which resulted in a L190P amino acid residue variation. This variant prevents Mocho de Espiga Branca from retrieving Na^+ from the root xylem leading to a high shoot Na^+ concentration. The identification of the tissue tolerant Mocho de Espiga Branca will accelerate the development of more elite salt tolerant bread wheat cultivars.

Keywords

Bread wheat, salt tolerance, *TaHKT1;5-D*, sodium, Na^+ transport, xylem sap Na^+, plant growth

Introduction

Globally, 45 million ha of irrigated and 32 million ha of dryland agricultural land is affected by salinity (FAO, 2019a). It is estimated that up to 1.2 million ha of land is lost to salinization each year (FAO, 2019a). To feed the rapidly growing human population, global food production must increase more than 70% by 2050, equating to an average increase of 44 million metric tons per year (Tester & Langridge, 2010). Bread wheat (*Triticum aestivum*) is the most widely cultivated cereal crop, in terms of area and provides one fifth of the total calories consumed worldwide (FAO, 2019b). Improving the salinity tolerance of bread wheat to maximise yields on saline agricultural land is required.

Salinity affects plants in two distinct stages. Shoot ion-independent stress (osmotic stress) arises immediately after plants are exposed to salt, inducing rapid physiological responses, such as stomatal closure and slower cell expansion, resulting in reduced plant growth (Munns & Tester, 2008). Shoot ion-dependent stress (ionic stress) has a slower onset and occurs when salt, particularly Na^+ and Cl^-, accumulate to high concentrations in the shoot (Munns & Tester, 2008). In this phase, reduced plant growth becomes more evident and premature leaf senescence occurs due to the toxicity of salt on cell metabolism (Munns & Tester, 2008).

Plants have three main mechanisms for tolerating salinity: osmotic stress tolerance via rapid, long distance signalling to maintain plant growth; ionic tissue tolerance by compartmentalising excessive Na^+ or Cl^- in vacuoles to avoid accumulation to toxic concentrations in the cytoplasm, and the exclusion of Na^+ from the shoot by retrieving Na^+ from the xylem into the root or through efflux of Na^+ into the soil to maintain a low shoot Na^+ concentration (Munns & Tester, 2008).

The High-Affinity Potassium Transporter 1;5 (HKT1;5) is known to be responsible for retrieving Na^+ from the transpiration stream in the root and preventing Na^+ from accumulating to high concentrations in the shoot (Hamamoto, Horie, Hauser, Deinlein, Schroeder & Uozumi, 2015). Plant HKT proteins belong to the high-affinity K^+/Na^+ transporting Ktr/TrK/HKT superfamily and are divided into two groups based on a serine/glycine substitution in the first loop of the proteins (Platten, Cotsaftis, Berthomieu, Bohnert, Davenport, Fairbairn, Horie, Leigh, Lin, Luan, Maser, Pantoja, Rodriguez-Navarro, Schachtman, Schroeder, Sentenac, Uozumi, Very, Zhu, Dennis & Tester, 2006). Members of the HKT1 group with a serine residue, typically transport Na^+, while the HKT2 group with a glycine side chain generally transport both Na^+ and K^+ (Platten *et al.*, 2006). In Arabidopsis (*Arabidopsis thaliana*) overexpression of *AtHKT1;1* in root stellar cells reduced shoot Na^+ accumulation by up to 64% compared to null segregants (Moller, Gilliham, Jha, Mayo, Roy, Coates, Haseloff & Tester, 2009). In bread wheat, the *AtHKT1;1* ortholog, *TaHKT1;5-D* reduces shoot Na^+ accumulation under salinity (Byrt, Xu, Krishnan, Lightfoot, Athman, Jacobs, Watson-Haigh, Plett, Munns, Tester & Gilliham, 2014). Durum wheat (*Triticum turgidum* L.), which lacks the D-genome accumulates high concentrations of Na^+ in the leaf (Munns, Rebetzke, Husain, James & Hare, 2003). However, when *TmHKT1;5-A* (*Nax2* locus) from a wheat relative *Triticum monococcum* L. was introduced into a commercial durum wheat, a reduction in leaf Na^+ concentration (James, Davenport & Munns, 2006) and a 25% improvement in grain yield in the field were observed (Munns, James, Xu, Athman, Conn, Jordans, Byrt, Hare, Tyerman, Tester, Plett & Gilliham, 2012).

Breeding of salt tolerant bread wheat cultivars has focused on selecting genotypes with improved shoot Na^+ exclusion (Ashraf & O'leary, 1996, Poustini & Siosemardeh, 2004). However, selection based on shoot Na^+ exclusion is not always correlated with increased

salinity tolerance in bread wheat (Genc, Oldach, Gogel, Wallwork, McDonald & Smith, 2013, Genc, Taylor, Lyons, Li, Cheong, Appelbee, Oldach & Sutton, 2019). Barley (*Hordeum vulgare* L.) is one of the most salt tolerant cereal crops and has much higher leaf Na^+ concentrations than bread wheat yet is able to maintain shoot growth in saline soils (Munns & Tester, 2008, Tilbrook, Schilling, Berger, Garcia, Trittermann, Coventry, Rabie, Brien, Nguyen & Tester, 2017). The identification of a bread wheat line that accumulates high shoot Na^+ concentrations whilst maintaining salinity tolerance, similar to barley, may accelerate the development of more salt tolerant bread wheat cultivars.

Here, we identified a Portuguese bread wheat landrace Mocho de Espiga Branca, which accumulated significantly higher leaf Na^+ concentrations while maintaining similar salinity tolerance as current commercial elite bread wheat cultivars. A naturally occurring single nucleotide polymorphism (SNP) in *TaHKT1;5-D* prevents Mocho de Espiga Branca from retrieving Na^+ from the root xylem, which results in a greater flux of Na^+ to the shoot and higher accumulation of Na^+ in leaf tissues.

Materials and Methods

Plant materials and growth condition

Two Australian commercial bread wheat cultivars Gladius and Scout and a set of 73 bread wheat diversity lines consisting of advanced cultivars, landraces and synthetic hexaploids were initially screened for salinity tolerance in this study (Garcia, Eckermann, Haefele, Satija, Sznajder, Timmins, Baumann, Wolters, Mather & Fleury, 2019). In the subsequent physiological characterizations, one of the 73 bread wheat diversity lines, a Portuguese landrace Mocho de Espiga Branca, and the commercial cultivars Gladius and Scout were

used. Plants in all the glasshouse experiments were grown under natural light with a daytime temperature at 22 °C and 15 °C at night.

Screening of bread wheat diversity set in a pot trial

A total of 75 lines (Gladius and Scout together with the 73 diversity lines) were screened for salinity tolerance in a fully automated conveyor system within a temperature controlled Smarthouse at the Australian Plant Phenomics Facility (The Plant Accelerator®, University of Adelaide, Australia; Latitude: -34.971366°, Longitude: 138.639758°) between August and September of 2014. Uniform sized seeds of each line were placed into 50 ml polypropylene tubes and imbibed in reverse osmosis (RO) water at room temperature for 4 h, tubes were drained and placed in the dark at 4 ºC for three days before sowing. 3 seeds from each line were sown in a free-draining plastic pot (145 mm diameter × 190 mm height) filled with 2.5 kg of a soil mixture (50% (v/v) University of California mix, 35% (v/v) peat mix and 15% (v/v) clay loam). The pots were arranged according to a split-plot experimental design with two consecutive pots forming a main plot. The lines were allocated to the main plots and were unequally replicated with Gladius and Scout replicated 12 times, 21 randomly-selected lines of the 73 diversity lines were replicated 4 times and the remaining 52 lines were replicated three times. The subplot design randomized the two treatment levels (0 and 100 mM NaCl) in each main plot. The main plot design was a blocked row-and-column design generated using DiGGer (Coombes, 2009) and the subplot randomization was generated using dae(Brien, 2014), packages for the R statistical computing environment (R Core Team, 2014). At the emergence of the 2nd leaf, plants were thinned to one uniformly sized plant per pot. At emergence of the 3rd leaf, pots were loaded onto an individual cart in the Smarthouse, where they were weighed daily and automatically watered to maintain the soil water content in each pot at 17% (w/w). At the emergence of the 4th leaf, 213 ml of either 0 or 170 mM

NaCl solution was applied to a saucer below each pot. Plants were not watered again until the soil water content reduced below 17% (w/w), and then each pot was watered again daily to maintain a final treatment concentration of 0 or 100 mM NaCl in the respective pot.

The shoot area of each plant was non-destructively imaged using a LemnaTec 3D Scanalyzer system (LemnaTec GmbH) for a total of 15 days (4 days before and 11 days after the NaCl treatment). Three red-green-blue (RGB) images (one top view and two side view images with a 90° angle) were recorded daily for each plant to calculate the projected shoot area (PSA) in pixels. 11 days after the NaCl treatment, the 4^{th} leaf blade of each plant was collected, weighed and dried in an oven at 60 °C for two days before the dry weight was recorded. The dried 4^{th} leaf blade was subsequently used for measuring Na^+, K^+ and Cl^- concentrations.

Determining leaf blade, leaf sheath and root Na^+ concentration in hydroponics

To measure the Na^+, K^+ and Cl^- concentrations in the 4^{th} leaf blade and sheath and roots, Mocho de Espiga Branca, Gladius and Scout were grown using a fully supported hydroponics system under three concentrations of NaCl (0, 150 and 200 mM) in a controlled glasshouse at The Plant Accelerator® between June and August 2017. The hydroponic system was equipped with a trolley fitted with two growth trays each containing 42 tubes filled with polycarbonate pellets and a tank containing 80 l of a modified Hoagland solution (mM): NH_4NO_3 (0.2); KNO_3 (5.0); $Ca(NO_3)_2{\cdot}4H_2O$ (2.0); $MgSO_4{\cdot}7H_2O$ (2.0); KH_2PO_4 (0.1); $Na_2Si_3O_7$ (0.5); NaFe(III)EDTA (0.05); $MnCl_2{\cdot}4H_2O$ (0.005); $ZnSO_4{\cdot}7H_2O$ (0.01); $CuSO_4{\cdot}5H_2O$ (0.0005) and $Na_2MoO_3{\cdot}2H_2O$ (0.0001). Uniform sized seeds from each genotype were surface sterilized using ultraviolet (UV) light for two min and germinated in petri dishes on moist filter paper for 4 days at room temperature before transplanting. 14 replicates from each cultivar were grown in each treatment trolley. The NaCl treatment was

applied at the emergence of the 4th leaf by adding 116.88 g of NaCl twice daily for a 25 mM NaCl increment until a final concentration of either 150 mM or 200 mM was reached, and no NaCl was added to the 0 mM NaCl treatment. 3.8 g of supplemental $CaCl_2 \cdot 2H_2O$ was added into the 150 and 200 mM NaCl treatment tanks at each 25 mM NaCl increment in order to maintain constant Ca^{2+} activity in all three treatments. The plants were irrigated by the nutrient solution in a 20 min flood and rain cycle and the complete nutrient solution was replaced every seven days. The pH of the solution was maintained between 6.5 and 7.0 throughout the experiment using a 3.2% (v/v) HCl solution and a portable waterproof specific Ion–pH–mV–Temperature meter (Modal WP-90, TPS Pty Ltd, Australia). After 21 days of NaCl treatment, the 4th leaf blade and sheath and the remaining shoots were sampled separately and weighed. Plant roots were weighed after sampling and approximately 5 cm of the root tip was used for RNA extraction. The roots from the 150 mM and 200 mM treatments were rinsed in 10 mM $CaSO_4$ solution and blotted on paper towel to remove traces of NaCl before sampling. The weighed 4th leaf blade, 4th leaf sheath, shoots and roots were dried in an oven at 60 °C for two days to record the dry weight. The dried 4th leaf blade and sheath and root tissue were used for the subsequent Na^+, K^+ and Cl^- concentration analysis.

Na^+, K^+ and Cl^- concentration analysis

The harvested dried 4th leaf blade and root samples were digested in 10 ml of 1% (v/v) HNO_3 (v/v), and the 4th leaf sheath was digested in 5 ml of 1% (v/v) HNO_3 (v/v) at 85 °C for 4 h in a SC154 HotBlock® (Environmental Express Inc., South Carolina, US). Na^+ and K^+ concentrations were measured using a flame photometer (Model 420; Sherwood Scientific Ltd., Cambridge, UK), and Cl^- concentration was measured using a chloride analyzer (Model 926; Sherwood Scientific Ltd., Cambridge, UK).

194 **RNA extraction and cDNA synthesis**

195 The harvested 5 cm root tips from the hydroponics experiment was snapped frozen in liquid
196 nitrogen and stored at -80 °C until RNA extraction. The root tissue was ground to a fine
197 powder using a 2010 Geno/Grinder® (SPEX SamplePrep) at 1000 ×g for 30 sec, and total
198 RNA was extracted from the tissue powder using a Direct-Zol RNA MiniPrep kit with DNase
199 I treatment (Zymo Research) according to the manufacturer's instruction. Final elution was
200 performed with 40 µl DNA/RNAase-Free water supplied and the eluted RNA was
201 subsequently quantified using a ND-1000 Spectrophotometer (NanoDrop Technologies) and
202 quantified on a 1% (w/v) agarose gel (Bioline) by electrophoresis. cDNA synthesis was
203 performed on 500 ng of RNA using High Capacity cDNA Reverse Transcription Kit (Thermo
204 Fisher Scientific) according to the manufacturer's instruction in a 20 µl reaction and stored at
205 -20 °C until use.

206

207 ***TaHKT1;5-D* coding sequence amplification and sequencing**

208 The entire coding sequence of the TaHKT1;5-D gene from Mocho de Espiga Branca, Gladius
209 and Scout were amplified using Phusion® High-Fidelity DNA polymerase (New England
210 Biolabs) following the manufacturer's instruction. The primers used for PCR amplification
211 were: forward primer *cTaHKT1;5-D_FP_1* (5'-ATGGGTTCTTTGCATGTCTCCT-3') and
212 reverse primer *cTaHKT1;5-D_RP_1551* (5'-TTATACTATCCTCCATGCCTCGC-3') (Table
213 S3). PCR was conducted on a T100™ Thermal Cycler (Bio-Rad) using the following
214 conditions: initial denaturation at 98 °C for 30 s, 35 cycles of 98 °C for 30 s, 64 °C for 30 s,
215 72 °C for 1 min, final extension at 72 °C for 10 min and held at 4 °C. The PCR product was
216 visualized on a 1% (w/v) agarose gel (Bioline) by electrophoresis at 90 V for 1 h and the 1.5
217 kb target band was collected for purification using NucleoSpin® Gel and PCR Clean-up kit
218 (Macherey-Nagel) according to the manufacturer's instruction prior to sequencing. Three

replicates from each of Mocho de Espiga Branca, Gladius and Scout TaHKT1;5-D coding sequence were tested with primers listed in Table S3 for Sanger sequencing carried out at the Australian Genome Research Facility (AGRF, South Australia).

***TaHKT1;5-D* gene expression in roots**

To determine *TaHKT1;5-D* expression in Mocho de Espiga Branca, Gladius and Scout, a PCR was conducted on the synthesised cDNA in a 25 µl reaction consisting of 1 µl cDNA, 0.5 µl each of 10 µM forward primer 5'-CGACCAGAAAAGGATAACAAGCAT-3' and reverse primer 5'-AGCCAGCTTCCCTTGCCAA-3', 5 µl *Taq* 5× Master Mix (New England Biolabs) and 18 µl Milli-Q water (18.2 MΩ cm). The final PCR products were visualized on a 1% (w/v) agarose gel (Bioline) by electrophoresis at 90 V for 1 h. The targeted *TaHKT1;5-D* product was 283 bp. The *TaGAP* gene (230 bp) was used as a positive control and a Milli-Q water sample was included as a negative control.

To quantify *TaHKT1;5-D* expression in the root tissue of Mocho de Espiga Branca, Gladius and Scout, Real-time PCR was performed on five replicates from each of the cultivars using an Applied Biosystems™ QuantStudio™ 6 Flex (Life Technologies). The reaction was performed in a 10 µl reaction consisting of two µL 1:20 diluted synthesised cDNA, 0.5 µl each of 10 µM forward and reverse primers stated above, 5 µl KAPA SYBR FAST 2× Master Mix (Sigma-Aldrich) and 2 µl Milli-Q water. The 283 bp final product from each cultivar was confirmed by Sanger sequencing carried out at AGRF (South Australia).

DNA extraction and quantification

Genomic DNA (gDNA) extraction of Mocho de Espiga Branca, Gladius, Scout and 70 bread wheat diversity lines was performed using a phenol/chloroform/iso-amyl alcohol extraction

method as described elsewhere with modifications (Rogowsky, Guidet, Langridge, Shepherd & Koebner, 1991). Briefly, the leaf tissue was frozen in a 10 ml tube at -80 °C and ground to a fine powder using a 2600 Cryo-Station (SPEX® SamplePrep) and a 2010 Geno/Grinder (SPEX® SamplePrep) at 1000 ×g for 30 s. 2 ml of gDNA extraction buffer [1% (w/v) sarkosyl, 100 mM Tris-HCl, 100 mM NaCl, 10mM EDTA, 2% (w/v) insoluble Polyvinyl-polypyrrolidone] was added to the ground tissue, vortexed, followed by the addition of 2 ml phenol/chloroform/iso-amyl alcohol (25:24:1). The sample was placed on ice for 20 min and vortexed thoroughly in every 5 min before centrifuging at 3630 ×g for 15 min. The supernatant was transferred into a labelled BD Vacutainer™ SST™ II Advance tube (Becton, Dickinson and Company, New Jersey, US) and 2 ml of phenol/chloroform/iso-amyl alcohol (25:24:1) was added. The sample was vortexed and centrifuged as above, and the supernatant was collected into a new 10 ml tube. The gDNA was precipitated using 2 ml of 100% (v/v) iso-propanol and 200 µl of 3 M sodium acetate (pH 4.8) and washed using 1 ml of 70% (v/v) ethanol before re-suspending overnight in 80 µl of R40 at 4°C. The re-suspended gDNA was quantified using a ND-1000 Spectrophotometer (NanoDrop Technologies).

Cleaved Amplified Polymorphic Sequence (CAPS) assay and genotyping

A CAPS marker tsl2SALTY-4D was designed to confirm the allele effect of the SNP (T/C) identified in Mocho de Espiga Branca *TaHKT1;5-D* for high leaf Na^+ concentration in comparison to Gladius and Scout. The extracted DNA from Mocho de Espiga Branca, Gladius, Scout and 68 bread wheat diversity lines were used for a PCR to amplify a 945 bp DNA fragment containing SNP. The PCR analysis was conducted in a 10 µl reaction consisting of 1 µg of DNA, 0.24 µl each of 10 µM forward primer 5'-ATGGGTTCTTTGCATGTCTCCT-3' and reverse primer 5'-CGCTAGCACGAACGCCG-3', 2 µl of *Taq* 5× Master Mix (New England Biolabs) and Milli-Q water. The reaction was

performed on a T100™ Thermal Cycler (Bio-Rad) using the following conditions: initial denaturation at 95 °C for 4 min, 35 cycles of 95 °C for 30 s, 56 °C for 30 s, 68 °C for 1 min, final extension at 68 °C for 5 min and held at 12 °C. The PCR amplification was followed by digestion using the restriction enzyme *FauI*. It was conducted in a 10 µl reaction consisting of 1 µg of the PCR products, 0.4 µl of *FauI* enzyme (New England Biolabs), 1 µl of 10× CutSmart® Buffer (New England Biolabs) and Milli-Q water. The digestion was performed on a T100™ Thermal Cycler (Bio-Rad) for 1 h at 55 °C followed by 20 min of inactivation at 65 °C and held at 12 °C. The digested product was visualized on a 2% (w/v) agarose gel (Bioline) by electrophoresis at 90 V for 90 min and the genotype of each line at the SNP position was confirmed according to the product bands on the gel. Lines which had the C:C genotype had two fragments present at 573 and 372 bp, whilst lines carrying the T:T genotype had a single fragment present.

Construction of 3D molecular models of TaHKT1;5-D and TaHKT1;5-D L190P

The most suitable template for wheat HKT1;5 transporter proteins was the *B. subtilis* KtrB K^+ transporter (Protein Data Bank accession 4J7C, chain I) (Vieira-Pires, Szollosi & Morais-Cabral, 2013) as previously identified (Xu, Waters, Byrt, Plett, Tyerman, Tester, Munns, Hrmova & Gilliham, 2018). The K^+ ion in KtrB was substituted by Na^+ during modelling of TaHKT1;5 proteins. 3D models of TaHKT1;5-D and TaHKT1;5-D L190P in complex with Na^+ were generated with Modeller 9v19 (Sali & Blundell, 1993) as described previously (Cotsaftis, Plett, Shirley, Tester & Hrmova, 2012, Waters, Gilliham & Hrmova, 2013) incorporating Na^+ ionic radii (Xu *et al.*, 2018) taken from the CHARMM force field (Brooks, Brooks, Mackerell, Nilsson, Petrella, Roux, Won, Archontis, Bartels, Boresch, Caflisch, Caves, Cui, Dinner, Feig, Fischer, Gao, Hodoscek, Im, Kuczera, Lazaridis, Ma, Ovchinnikov, Paci, Pastor, Post, Pu, Schaefer, Tidor, Venable, Woodcock, Wu, Yang, York & Karplus,

2009), on the Linux station running the Ubuntu 12.04 operating system. Best scoring models (from an ensemble of 50) were selected based on the combination of Modeller Objective (Shen & Sali, 2006) and Discrete Optimised Protein Energy (Eswar, Eramian, Webb, Shen & Sali, 2008) functions, PROCHECK (Laskowski, Macarthur, Moss & Thornton, 1993), ProSa 2003(Sippl, 1993) and FoldX (Schymkowitz, Rousseau, Martins, Ferkinghoff-Borg, Stricher & Serrano, 2005). Structural images were generated in the PyMOL Molecular Graphics System V1.8.2.0 (Schrődinger LLC, Portland, OR, USA). Calculations of angles between selected α-helices in HKT1;5 models were executed in Chimera (Pettersen, Goddard, Huang, Couch, Greenblatt, Meng & Ferrin, 2004) and evaluations of differences ($\Delta\Delta G = \Delta G_{mut} - \Delta G_{wt}$) of Gibbs free energies was performed with FoldX (Schymkowitz *et al.*, 2005). Sequence conservation patterns were analysed with ConSurf (Celniker, Nimrod, Ashkenazy, Glaser, Martz, Mayrose, Pupko & Ben-Tal, 2013, Landau, Mayrose, Rosenberg, Glaser, Martz, Pupko & Ben-Tal, 2005) based on 3D models of TaHKT1;5-D using 370 sequences at the sequence identities of 30% and higher (specifications: HMMMER homolog search algorithm, UNIREF-90 Protein database with the E-value cut-off of 1×10^{-4}, Bayesian Model of substitution for proteins.

Characterization of TaHKT1;5-D from Mocho de Espiga Branca and Gladius in *X. laevis* oocytes

Na^+ transport properties of TaHKT1;5-D from Mocho de Espiga Branca and Gladius were characterized in *X. laevis* oocytes using two-electrode voltage clamping (TEVC) as previously described (Byrt *et al.*, 2014, Munns *et al.*, 2012). pGEMHE-DEST containing *TaHKT1;5-D* was linearized using sbfI-HF (New England Biolabs) before synthesising cRNA using the mMESSAGE mMACHINE T7 Kit (Ambion) following manufacturer's instructions. 46 nl/23 ng of the cRNA from Mocho de Espiga Branca or Gladius, or equal

319 volumes of RNA-free water (H_2O control) were injected into oocytes. Injected oocytes were
320 incubated for 48 h and TEVC was carried out as described (Munns *et al.*, 2012). Membrane
321 currents were recorded in the HMg solution (6 mM $MgCl_2$, 1.8 mM $CaCl_2$, 10 mM MES, and
322 pH 6.5 adjusted with a Tris base) ± Na^+ glutamate. The osmolality of the solution was
323 adjusted to 240 - 260 mOsmol/Kg using mannitol and a micro-osmometer (Model 210, Fiske
324 Associates Inc, USA).
325
326 **Subcellular localisation of TaHKT1;5-D**
327 Transient expression of fluorescent fusion proteins was performed as previously described
328 (Henderson, Wege, Qiu, Blackmore, Walker, Tyerman, Walker & Gilliham, 2015). In brief,
329 *TaHKT1;5-D* coding sequences of Mocho de Espiga Branca and Gladius were recombined
330 into pMDC43 (Curtis & Grossniklaus, 2003) to generate N-terminally green fluorescent
331 protein (GFP) tagged proteins. The red fluorescent protein (RFP) tagged plasma membrane
332 marker nCBL1-RFP that was used for co-localisation (Batistic, Sorek, Schultke, Yalovsky &
333 Kudla, 2008). All constructs were transformed into *Agrobacterium tumefaciens* strain Agl-1
334 and agro-infiltration was performed on fully expanded leaves of 4 to 6 weeks old tobacco
335 (*Nicotiana benthamiana*) plants (Henderson *et al.*, 2015). After two to three days, leaf
336 sections were imaged using a Nikon A1R Confocal Laser-Scanning Microscope equipped
337 with a 63× water objective lens and NIS-Elements C software (Nikon Corporation).
338 Excitation/emission conditions were GFP (488 nm/500–550 nm) and RFP (561 nm/570–620
339 nm).
340
341 **Xylem sap Na^+ and K^+ concentration analysis**
342 Xylem sap was collected from hydroponically grown plants of Mocho de Espiga Branca and
343 Gladius at 0 and 150 mM NaCl after 21 days from the start of the NaCl treatment. The shoot

was cut off at the base of the plant and inserted into a Scholander-type pressure chamber (Model 1005, PMS Instrument Company, USA) to extrude the xylem sap by slowly filling the chamber with compressed air. The sap was immediately collected into a clean, pre-weighed 1.5 ml tube. From the 0 mM NaCl treatment, xylem sap of seven plants from each cultivars was collected, and xylem sap of eight Mocho de Espiga Branca and seven Gladius plants was collected from the 150 mM NaCl treatment. Tubes containing the xylem sap was weighed for each plant and the samples were stored at 4°C until Na^+ and K^+ concentrations were measured using a flame photometer (Model 420, Sherwood Scientific Ltd., Cambridge, UK).

Net and total Na^+, K^+ and H^+ flux analyses using Microelectrode Ion Flux Estimation (MIFE)

To investigate whether there were differences in Na^+, K^+ and H^+ transport in the plant roots between Mocho de Espiga Branca and Gladius, net fluxes of Na^+, K^+ and H^+ were measured at root maturation and elongation zones using the non-invasive MIFE technique (University of Tasmania, Hobart, Australia) (Bose, Rodrigo-Moreno, Lai, Xie, Shen & Shabala, 2015, Newman, 2001).

Root Na^+ retrieval measurements were performed at the elongation zone (approximately 600 µm from the root cap). Uniform sized sterilized seeds from Mocho de Espiga Branca and Gladius were germinated on moist filter paper in Petri dishes covered with aluminium foil, at 4 °C overnight and then placed at room temperature in the dark for three days before transplanting. 12 seedlings from each cultivar were transplanted into a hydroponic tank containing 10 L modified Hoagland solution as previously described. NaCl was added into the solution at an increment of 25 mM (14.16 g) twice daily for two days to achieve a final concentration of 100 mM NaCl. The pH of the solution was maintained between 6.5 and 7.0

throughout the experiment using 3.2% (v/v) of the HCl solution and a portable waterproof specific Ion–pH–mV–Temperature meter (Modal WP-90, TPS Pty Ltd, Australia). Two days after being exposed to 100 mM NaCl, the entire roots of Mocho de Espiga Branca (n = 9) and Gladius (n = 8) were first preconditioned in BSM solution containing 100 mM NaCl (0.2 mM KCl + 0.1 mM $CaCl_2 \cdot 2H_2O$ + 100 mM NaCl) in a Petri dish for 30 min and then the primary root was immobilized on a 10 ml perspex measuring chamber containing 7 ml of the same BSM medium. The steady-state fluxes were measured for 5 min in the initial BSM solution before changing the bathing solution to 7 ml of the new BSM medium solution containing 0.6 mM NaCl (0.2 mM KCl + 0.1 mM $CaCl_2 \cdot 2H_2O$ + 0.6 mM NaCl). The resulting fluxes were measured for 25 min and the integral of each replication was added to derive the cumulative total fluxes. The osmolality of the two BSM solutions and the Hoagland solution were maintained between 208 and 222 mOsmol/kg using mannitol and a vapour pressure osmometer (Model 5500, Wescor, Inc., USA).

Root Na^+ uptake measurements were performed at the maturation zone (beyond 2.5 cm from root tip), uniform sized sterilized seeds were germinated as described above, placed at 4 °C overnight and placed at room temperature in the dark for three days before measurement. The primary root of Mocho de Espiga Branca (n = 12) and Gladius (n = 11) seedlings was immobilized on a 10 ml perspex measuring chamber containing 6 ml of the BSM solution (0.2 mM KCl + 0.1 mM $CaCl_2 \cdot 2H_2O$ + 0.6 mM NaCl) and pre-conditioned for 20 min before recording steady-state Na^+, K^+ and H^+ fluxes for 5 min then 100 mM NaCl was added and the resulting fluxes were recorded for 25 min.

Statistical analysis

Prism 7 for Windows (version 7.02; GraphPad Software, Inc.) was used to generate graphs. GenStat® 15th edition for Microsoft Windows (version 15.3.09425; VSN International Ltd, UK) was used to perform an Analysis of Variance (ANOVA) and Tukey's multiple comparison test was used to determine which means were significantly different at a probability level of $p \leq 0.05$.

Results

Mocho de Espiga Branca has high leaf and sheath Na^+ concentrations

Screening of 75 bread wheat accessions for salinity tolerance under 100 mM NaCl, identified a Portuguese landrace, Mocho de Espiga Branca, which had a similar salinity tolerance but accumulated 7 folds higher Na^+ concentration in the 4th leaf compared to all other lines, including Gladius and Scout (Figure 1 and Table S1). The 4th leaf K^+ and Cl^- concentrations of the 75 wheat lines were comparable under 100 mM NaCl (Table S1).

In hydroponics, Mocho de Espiga Branca maintained a similar shoot and root biomass to Gladius and Scout at 0, 150 and 200 mM NaCl (Figure 2a and Figure S1a,b), and all three cultivars had comparable salinity tolerance at 150 mM (0.69, 0.64 and 0.60, respectively) and 200 mM NaCl (0.39, 0.49 and 0.39, respectively) (Figure S1c,d). The 4th leaf blade and sheath Na^+ concentrations were up to 6 folds higher in Mocho de Espiga Branca than Gladius and Scout at 150 mM NaCl (Figure 2b,c). At 200 mM NaCl, 4th leaf blade and sheath Na^+ concentrations in Mocho de Espiga Branca were 5 folds greater compared to Gladius and Scout (Figure 2b,c). There was no difference in root Na^+ concentration at all NaCl treatments (Figure 2d).

All three cultivars had similar K^+ concentrations in the 4th leaf blade and sheath under 0 mM NaCl (Figure S2a). At 150 and 200 mM NaCl, Mocho de Espiga Branca accumulated 70-79% less K^+ in the blade and 61-67% less K^+ in the sheath compared to Gladius and Scout (Figure S2a, b). The root K^+ concentration in Mocho de Espiga Branca was similar to Scout but significantly lower than Gladius under 0 mM NaCl, while no differences were observed between the three cultivars under 150 and 200 mM NaCl (Figure S2c).

The 4th leaf blade and sheath Cl^- concentrations in Mocho de Espiga Branca, Gladius and Scout were similar under 0 mM NaCl (Figure S2d,e). Mocho de Espiga Branca accumulated significantly higher Cl^- than Gladius and Scout in both tissues under 150 and 200 mM NaCl (Figure S2d,e). There were no significant differences in root Cl^- concentrations at 0 mM NaCl (Figure S2f). Mocho de Espiga Branca had significantly higher Cl^- than Gladius and Scout at 150 mM NaCl but only significantly higher than Scout at 200 mM NaCl (Figure S2f).

A natural single nucleotide substitution in the *TaHKT1;5-D* gene of Mocho de Espiga Branca alters Na^+ transport properties of the protein

A natural single SNP (T/C) in the coding sequence of *TaHKT1;5-D* was identified at the 569th base pair in Mocho de Espiga Branca, while the sequence of Gladius and Scout was identical to Chinese Spring (Figure 3a). The SNP in Mocho de Espiga Branca resulted in an amino acid residue change from Leucine (L) to Proline (P) at the 190th residue in the Na^+ transporter protein TaHKT1;5-D (Figure 3a). This L190P variant residue is predicted to be located on the 4th transmembrane α-helix in the area of the second glycine residue of the S78-G233-G353-G457 selectivity filter motif (Figure 3b). Expression analysis of the *TaHKT1;5-D* in Mocho de Espiga Branca, Gladius and Scout showed no significant difference in expression (Figure S3a,b). A cleaved amplified polymorphic sequence (CAPS) marker

444 tsl2SALTY-4D designed to this SNP in *TaHKT1;5-D* was used to genotype 71 diversity lines
445 (Figure S3c and Table S2). Mocho de Espiga Branca carried the C:C allele responsible for the
446 TaHKT1;5-D L190P variation, while all other lines had the T:T allele as Gladius and Scout
447 (Figure S3c and Table S2).
448
449 3D molecular modelling revealed that overall folds of TaHKT1;5-D and TaHKT1;5-D L190P
450 were similar (Figure 3c,d). Detailed analysis of the microenvironments around α-helix 4 and
451 α-helix 5 (two black arrows pointing to each other in Figure 3d), revealed that L190 in α-
452 helix 4 of TaHKT1;5-D (Figure 3d left) established four polar contacts at separations
453 between 2.6 Å to 3.2 Å with V186, V187, Y193 and S194 neighbouring residues. These
454 extensive polar contacts were not formed in the TaHKT1;5-D L190P variant (Figure 3d right),
455 which only established one polar contact at the separation at 2.7 Å. In TaHKT1;5-D, the
456 packing angle between α-helix 4 (carrying L190P) and the neighbouring α-helix 5 was 16°
457 sharper than that in TaHKT1;5D L190P (Figure 3d). Sequence conservation patterns, based
458 on 3D models of TaHKT1;5-D revealed that the P190 position in TaHKT1;5-D could not be
459 found in databases, meaning that L190 could only be replaced by F, G, L, V, I, M, A, K and
460 T, but not by P. Evaluation of differences of Gibbs free energies of TaHKT1;5-D revealed
461 that the L190P mutation was energetically highly unfavourable (highly destabilising), and
462 that the reverse mutation (P190 into L190) restored 70% of this energy loss.
463
464 To examine the effect of the L190P variant in the Na^+ transport properties of the TaHKT1;5-
465 D transporter, *TaHKT1;5-D* cRNA from Mocho de Espiga Branca or Gladius was introduced
466 in *X. laevis* oocytes. When exposed to different concentrations of Na^+ glutamate (1 and 30
467 mM Na^+), the oocytes with *TaHKT1;5-D* from Gladius had a significantly higher Na^+ elicited
468 inward current, whereas those with *TaHKT1;5-D* from Mocho de Espiga Branca had limited

current, similar to the H_2O-injected oocytes (Figure 4a). The TaHKT1;5-D from Gladius showed a positive reversal potential shift when exposed to 30 mM Na^+ which was not observed with TaHKT1;5-D L190P from Mocho de Espiga Branca (Figure 4a).

Transient expression of N-terminally GFP-tagged TaHKT1;5-D variants in *Nicotiana benthamiana* leaves revealed differences in GFP-signal pattern (Figure 4b). The majority of GFP-TaHKT1;5-D signal co-localised with the plasma membrane (PM) marker CBL1n-RFP, and a minor fraction to mobile subcellular organelles (Figure 4b). GFP-signal in leaves infiltrated with GFP-TaHKT1;5-D L190P, however, localised to internal cell structures, including a faint cytosolic signal and brighter non-mobile structures (Figure 4b). Suggesting the TaHKT1;5-D L190P might get degraded; possibly due to instability of the protein as revealed by homology modelling.

The Na^+ transport properties of the TaHKT1;5-D L190P variant was further investigated by comparing the xylem sap Na^+ concentrations of Mocho de Espiga Branca and Gladius grown hydroponically under 0 and 150 mM NaCl. Mocho de Espiga Branca accumulated a 3.5 folds greater xylem sap Na^+ than Gladius at 150 mM NaCl, while no significant differences were observed at 0 mM NaCl (Figure 4c). There was no significant difference for xylem sap K^+ and Cl^- concentrations for either cultivar (Figure S4a,b).

The ability of Mocho de Espiga Branca to influx or efflux Na^+ at the root elongation zone was assessed in five day old seedlings using a basal salt medium (BSM) with ion fluxes monitored for 25 min. In the first minute after being exposed to 0.6 mM NaCl, Mocho de Espiga Branca and Gladius had an increase in net Na^+ efflux up to 10000 and 35000 nmol/m^2 s^1 respectively compared to the BSM with 100 mM NaCl (Figure 5a). However, Mocho de

Espiga Branca changed within the first minute to Na^+ influx, while Gladius maintained Na^+ efflux for the duration of measurement (Figure 5a). The transient net K^+ efflux was greater in Mocho de Espiga Branca than Gladius and the efflux rates gradually dropped to below 1000 nmol/m^2 s^1 in both cultivars (Figure 5b). Mocho de Espiga Branca had a net H^+ influx for 25 min, while Gladius initially became a net influxer for 8 min and then reverted to being a net effluxer for the remainder of the experiment after exposure to 0.6 mM Na^+ (Figure 5c). Overall, Mocho de Espiga Branca had greater total Na^+ influx, K^+ efflux and H^+ influx compared to Gladius at the root elongation zone (Figure 5 d,e,f).

In contrast, both cultivars had net Na^+ influx for the first few minutes followed by a gradual net efflux at the maturation zone of the primary root (Figure S5a). As expected salt stress induced K^+ efflux in both cultivars (Figure S5b). However, there was no significant difference in net or total Na^+ and K^+ fluxes observed between the two cultivars, while Mocho de Espiga Branca had 2 folds greater net H^+ efflux than Gladius (Figure S5 a-f).

Discussion

A bread wheat landrace, Mocho de Espiga Branca, was identified with significantly higher leaf Na^+ concentrations and the ability to maintain growth under high salinity. DNA sequencing revealed a naturally occurring SNP in the coding region of the Na^+ transporter TaHKT1;5-D, resulting in a L190P amino acid residue change. This variation disrupted the capability of TaHKT1;5-D to retrieve Na^+ from the xylem, due to the protein being unable to transport Na^+ and/or degradation of the TaHKT1;5-D L190P variant.

3D structural modelling of TaHKT1;5-D and TaHKT1;5-D L190P revealed the important role of the L190P substitution in determining the functional properties of Na^+ transport in

TaHKT1;5-D. The lack of the cooperative binding networks around α-helix 4 of TaHKT1;5-D L190P within the P190 environment (Figure 3d) imposes a severe structural rigidity on the 3D folding of this transporter. The more obtuse packing angle between α-helix 4 and α-helix 5 of TaHKT1;5-D L190P compared to that in TaHKT1;5-D, indicated that the proline position affects packing of α-helices in this specific environment (Figure 3d). Therefore, this α-helix is unlikely to function properly in the structural context preventing Na^+ ion conductance. In TaHKT1;5-D, a positive correlation was identified between structural characteristics of α-helix 4 and α-helix 5 (trends in angles based on α-helical planes), differences in Gibbs free energies of forward (L190P) and reverse (P190L) mutations and the ability to conduct Na^+. The inability of the Mocho de Espiga Branca L190P variant to transport Na^+ was confirmed by expressing the gene in *X. laevis* oocytes (Figure 4a).

Studies also identified differences between the location of the Mocho de Espiga Branca L190P variant and common TaHKT1;5-D. Unlike common TaHKT1;5-Ds, which are localised on the plasma membrane of stelar cells, the L190P variant exhibited greater localisation of GFP signal in internal, non-moving structures (Figure 4b), suggesting the protein is being retained internally and/or is being targeted for degradation. Whether the TaHKT1;5-D L190P is functional and/or not on the correct membrane, Mocho de Espiga Branca will not be able retrieve Na^+ from the xylem (Figure 4c), explaining why this accession has high leaf blade and leaf sheath Na^+ (Figure 2b,c).

This work is, to our knowledge, the first that shows a naturally occurring mutation in *TaHKT1;5* directly effects both the Na^+ transport properties of the protein and the plant phenotype. Previously, differences in the amino acid sequences between Nipponbare and Pokkali *OsHKT1;5* were hypothesised to be responsible for differences in shoot Na^+

accumulation, however, the transport properties of these proteins were not directly tested (Cotsaftis *et al.*, 2012), a similar observation was recently made in barley (van Bezouw, Janssen, Ashrafuzzaman, Ghahramanzadeh, Kilian, Graner, Visser & van der Linden, 2019). Similarly artificially induced mutations in TmHKT1;5-A, which occurred during cloning of the gene, were shown to disrupt Na^+ transport properties in *X. laevis* but this was not linked to a plant phenotype (Xu *et al.*, 2018). A similar natural HKT1;5 variant (L189P) has recently been identified in barley accessions accumulating high grain Na^+ concentration, which also lacked the ability to transport Na^+ in *X. laevis* oocytes and was similarly shown to be on internal subcellular structures (Houston et al. unpublished).

Both Mocho de Espiga Branca and Gladius had similar concentrations of K^+ in the xylem sap (Figure S4a), however Mocho de Espiga Branca accumulated less K^+ in the leaf blade and sheath (Figure S2a,b). The greater K^+ efflux at the root elongation zone in Mocho de Espiga Branca (Figure 5b,e) suggests the significant reduction in K^+ in the leaf blade and sheath is associated with increased K^+ leakage from the roots. Root Na^+ and K^+ concentrations were similar between the two cultivars (Figure 2d and Figure S2c), even though there was a greater root Na^+ influx (Figure 5a,d), increased shoot Na^+ (Figure 2b,c), a higher root K^+ efflux (Figure 5b,e) and reduced shoot K^+ (Figure S2a,b) in Mocho de Espiga Branca. Bread wheat may have a mechanism, which enables the maintenance of optimal root Na^+ and K^+ concentrations contributing to the tolerance of the whole plant to salinity stress. In both cultivars, a high concentration of Cl^- was transported in the xylem sap (Figure S4b), which accumulated in the leaf sheath to a greater extent than the leaf blade (Figure S2d,e). This is in agreement with previous findings of Cl^- partitioning into the leaf sheath in response to salinity and suggests that the leaf sheath may have an important role in Cl^- exclusion

preventing it from accumulating to toxic concentrations in the leaf blade (Boursier & Läuchli, 1989, Boursier, Lynch, Lauchli & Epstein, 1987).

Based on the observed functional defects in Na^+ transport resulting from the TaHKT1;5-D L190P variant and the ion analysis findings in this study, we propose a model to compare root-to-shoot ion transport between Mocho de Espiga Branca and Gladius (Figure 6). Due to the naturally occurring SNP in *TaHKT1;5-D*, we suggest that Mocho de Espiga Branca has impaired retrieval of Na^+ from the root xylem which results in a greater influx of Na^+ in the xylem sap and a higher accumulation in the leaf blade and sheath compared to Gladius (Figure 6).

The results of this study confirm the importance of *TaHKT1;5-D* in the Na^+ exclusion mechanism of bread wheat to limit the levels of Na^+ that accumulate. It is evident, however, that *TaHKT1;5-D* does not represent the only mechanism responsible for the salinity tolerance of a whole plant, as Mocho de Espiga Branca maintained similar tolerance to Gladius and Scout despite carrying the non-functional *TaHKT1;5-D*. It appears that although *TaHKT1;5-D* has a key role in Na^+ exclusion, salinity tolerance in bread wheat may not necessarily be entirely related to the plants ability to maintain a low shoot Na^+ concentration. The lack of a relationship between shoot Na^+ concentration and salinity tolerance in bread wheat has been observed in other studies (Genc, McDonald & Tester, 2007, Genc *et al.*, 2019). This raises the question of how Mocho de Espiga Branca and these other bread wheat accessions maintain growth despite accumulating a high concentration of shoot Na^+? There must be other tolerance mechanisms, such as tissue tolerance, that are responsible for the plant's ability to tolerate high shoot Na^+ concentrations under salinity. Tissue tolerance mechanisms, such as vacuolar Na^+ compartmentation, the synthesis of compatible solutes and

592 production of enzymes responsible for reactive oxygen species (ROS) metabolism are
593 reported to be essential in plant growth maintenance (Flowers & Colmer, 2008, Munns &
594 Tester, 2008). Specific signalling pathway mechanisms, such as those for ROS, which have
595 been shown to play a role in regulating vasculature Na^+ concentrations (Mittler,
596 Vanderauwera, Suzuki, Miller, Tognetti, Vandepoele, Gollery, Shulaev & Van Breusegem,
597 2011, Suzuki, Koussevitzky, Mittler & Miller, 2012), or Ca^{2+} pathways, which regulate gene
598 expression and protein activities (Kudla, Batistič & Hashimoto, 2010, Thoday-Kennedy,
599 Jacobs & Roy, 2015), could also be important for the plant and/or cell's ability to tolerate
600 high concentrations of shoot Na^+. Therefore, future studies towards improving salinity
601 tolerance of bread wheat should focus on identifying genetics and physiological mechanisms
602 involved in the plant's tolerance to high shoot Na^+ (tissue tolerance) rather than preferentially
603 focusing on Na^+ exclusion. This will now be easier, knowing it is possible for wheat to
604 survive high shoot Na^+ concentrations.
605
606 In summary, this study identified a bread wheat landrace, Mocho de Espiga Branca, that
607 maintains shoot growth while accumulating very high leaf Na^+ concentrations under salinity -
608 a novel bread wheat line with tissue tolerance. A naturally occurring SNP variation in the
609 coding region of *TaHKT1;5-D* of Mocho de Espiga Branca results in the amino acid residue
610 substitution L190P in the Na^+ transporter TaHKT1;5-D, and this single substitution appeared
611 to negatively affect the Na^+ transport function of the protein, which results in high leaf Na^+
612 concentrations. Access to both Mocho de Espiga Branca and the CAPS marker tsl2SALTY-
613 4D for tracking the SNP variation in TaHKT1;5-D will enable plant breeders to develop
614 salinity tolerant bread wheat varieties in the future.
615
616

Acknowledgements

This project was funded by the Grains Research and Development Corporation (GRDC): Project UA00145, UA00151, and the GRDC and the International Wheat Yield Partnership (IWYP): Projects IWYP39/ACP0009; IWYP60/ANU00027. The Australian Centre for Plant Functional Genomics (ACPFG) was jointly funded by the Australian Research Council (ARC) and the GRDC, SW was supported by the ARC DE160100804. The Plant Accelerator®, Australian Plant Phenomics Facility, is funded under the National Collaborative Research Infrastructure Strategy (NCRIS). We acknowledge the Cereal Genetic Resource Centre (GRC) INRA Clermont-Ferrand, Assoc. Prof. Kenneth Chalmers and Dr. Melissa Garcia for providing seeds. We thank The Plant Accelerator® for assisting with the glasshouse experiments and Adelaide microscopy for assistance with imaging. We also thank Prof. Rana Munns (CSIRO, Black Mountain, Canberra and University of Western Australia, Perth, Australia) for valuable comments and discussion on the manuscript. CB thanks the China Scholarship Council and the University of Adelaide Joint Postgraduate Scholarships Program for her PhD stipend, and acknowledges the Research Travel Scholarship and the Global Learning Travel Grant at the University of Adelaide and The Plant Nutrition Trust for financial support to attend conferences. The authors declare that they have no conflict of interest.

References

Ashraf M. & O'leary J. (1996). Responses of some newly developed salt-tolerant genotypes of spring wheat to salt stress: 1. Yield components and ion distribution. *Journal of Agronomy and Crop Science*, 176, 91-101.

Batistic O., Sorek N., Schultke S., Yalovsky S. & Kudla J. (2008). Dual fatty acyl modification determines the localization and plasma membrane targeting of CBL/CIPK Ca^{2+} signaling complexes in *Arabidopsis*. *The Plant Cell*, 20, 1346-1362.

Bose J., Rodrigo-Moreno A., Lai D., Xie Y., Shen W. & Shabala S. (2015). Rapid regulation of the plasma membrane H^{+}-ATPase activity is essential to salinity tolerance in two halophyte species, *Atriplex lentiformis* and *Chenopodium quinoa*. *Annals of Botany*, 115, 481-494.

Boursier P. & Läuchli A. (1989). Mechanisms of chloride partitioning in the leaves of salt-stressed *Sorghum bicolor* L. *Physiologia Plantarum*, 77, 537-544.

Boursier P., Lynch J., Lauchli A. & Epstein E. (1987). Chloride partitioning in leaves of salt-stressed sorghum, maize, wheat and barley. *Functional Plant Biology*, 14, 463-473.

Brien C. (2014). Dae: Functions useful in the design and ANOVA of experiments. R package version 2.3-1.

Brooks B.R., Brooks C.L., Mackerell A.D., Nilsson L., Petrella R.J., Roux B., Won Y., Archontis G., Bartels C., Boresch S., Caflisch A., Caves L., Cui Q., Dinner A.R., Feig M., Fischer S., Gao J., Hodoscek M., Im W., Kuczera K., Lazaridis T., Ma J., Ovchinnikov V., Paci E., Pastor R.W., Post C.B., Pu J.Z., Schaefer M., Tidor B., Venable R.M., Woodcock H.L., Wu X., Yang W., York D.M. & Karplus M. (2009). CHARMM: The biomolecular simulation program. *Journal of Computational Chemistry*, 30, 1545-1614.

660 Byrt C.S., Xu B., Krishnan M., Lightfoot D.J., Athman A., Jacobs A.K., Watson-Haigh N.S.,
661 Plett D., Munns R., Tester M. & Gilliham M. (2014). The Na^+ transporter, TaHKT1;5-
662 D, limits shoot Na^+ accumulation in bread wheat. *The Plant Journal*, 80, 516-526.
663 Celniker G., Nimrod G., Ashkenazy H., Glaser F., Martz E., Mayrose I., Pupko T. & Ben-Tal
664 N. (2013). ConSurf: Using evolutionary data to raise testable hypotheses about protein
665 function. *Israel Journal of Chemistry*, 53, 199-206.
666 Coombes N. (2009). DiGGer design search tool in R. In: *New South Wales Department of*
667 *Primary Industry) Available at* http://nswdpibiom.org/austatgen/software/ *[Verified 29*
668 *August 2017]*.
669 Cotsaftis O., Plett D., Shirley N., Tester M. & Hrmova M. (2012). A two-staged model of
670 Na^+ exclusion in rice explained by 3D modeling of HKT transporters and alternative
671 splicing. *PLoS ONE*, 7, e39865.
672 Curtis M.D. & Grossniklaus U. (2003). A gateway cloning vector set for high-throughput
673 functional analysis of genes in planta. *Plant Physiology*, 133, 462-469.
674 Eswar N., Eramian D., Webb B., Shen M.-Y. & Sali A. (2008). Protein structure modeling
675 with MODELLER. In: *Structural Proteomics: High-Throughput Methods* (eds B. Kobe,
676 M. Guss, & T. Huber), pp. 145-159. Human Press, Totowa, NJ.
677 FAO (2019a). FAO Soils portal. *Available at* http://www.fao.org/soils-portal/soil-
678 management/management-of-some-problem-soils/salt-affected-soils/more-information-
679 on-salt-affected-soils/en/ *[Accessed 26 May 2019]*.
680 FAO (2019b). FAOSTAT. *Available at* http://www.fao.org/faostat/en/#data/QC *[Accessed*
681 *26 May 2019]*.
682 Flowers T.J. & Colmer T.D. (2008). Salinity tolerance in halophytes. *New Phytologist*, 179,
683 945-963.

684 Garcia M., Eckermann P., Haefele S., Satija S., Sznajder B., Timmins A., Baumann U.,
685 Wolters P., Mather D.E. & Fleury D. (2019). Genome-wide association mapping of
686 grain yield in a diverse collection of spring wheat (*Triticum aestivum* L.) evaluated in
687 southern Australia. *PLoS ONE*, 14, e0211730.
688 Genc Y., McDonald G.K. & Tester M. (2007). Reassessment of tissue Na^+ concentration as a
689 criterion for salinity tolerance in bread wheat. *Plant Cell and Environment*, 30, 1486-
690 1498.
691 Genc Y., Oldach K., Gogel B., Wallwork H., McDonald G.K. & Smith A.B. (2013).
692 Quantitative trait loci for agronomic and physiological traits for a bread wheat
693 population grown in environments with a range of salinity levels. *Molecular Breeding*,
694 32, 39-59.
695 Genc Y., Taylor J., Lyons G.H., Li Y., Cheong J., Appelbee M., Oldach K. & Sutton T.
696 (2019). Bread wheat with high salinity and sodicity tolerance. *Frontiers in Plant*
697 *Science*, 10, 1280.
698 Hamamoto S., Horie T., Hauser F., Deinlein U., Schroeder J.I. & Uozumi N. (2015). HKT
699 transporters mediate salt stress resistance in plants: from structure and function to the
700 field. *Current Opinion in Biotechnology*, 32, 113-120.
701 Henderson S.W., Wege S., Qiu J., Blackmore D.H., Walker A.R., Tyerman S.D., Walker R.R.
702 & Gilliham M. (2015). Grapevine and arabidopsis cation-chloride cotransporters
703 localize to the golgi and trans-golgi network and indirectly influence long-distance ion
704 transport and plant salt tolerance. *Plant Physiology*, 169, 2215-2229.
705 James R.A., Davenport R.J. & Munns R. (2006). Physiological characterization of two genes
706 for Na^+ exclusion in durum wheat, *Nax1* and *Nax2*. *Plant Physiology*, 142, 1537-1547.
707 Kudla J., Batistič O. & Hashimoto K. (2010). Calcium signals: the lead currency of plant
708 information processing. *The Plant Cell*, 22, 541-563.

709 Landau M., Mayrose I., Rosenberg Y., Glaser F., Martz E., Pupko T. & Ben-Tal N. (2005).
710 ConSurf 2005: the projection of evolutionary conservation scores of residues on protein
711 structures. *Nucleic Acids Research*, 33, W299-W302.
712 Laskowski R.A., Macarthur M.W., Moss D.S. & Thornton J.M. (1993). PROCHECK: a
713 program to check the stereochemical quality of protein structures. *Journal of Applied*
714 *Crystallography*, 26, 283-291.
715 Mittler R., Vanderauwera S., Suzuki N., Miller G., Tognetti V.B., Vandepoele K., Gollery M.,
716 Shulaev V. & Van Breusegem F. (2011). ROS signaling: the new wave? *Trends in*
717 *Plant Science*, 16, 300-309.
718 Moller I.S., Gilliham M., Jha D., Mayo G.M., Roy S.J., Coates J.C., Haseloff J. & Tester M.
719 (2009). Shoot Na^+ exclusion and increased salinity tolerance engineered by cell type-
720 specific alteration of Na^+ transport in *Arabidopsis*. *The Plant Cell*, 21, 2163-2178.
721 Munns R., James R.A., Xu B., Athman A., Conn S.J., Jordans C., Byrt C.S., Hare R.A.,
722 Tyerman S.D., Tester M., Plett D. & Gilliham M. (2012). Wheat grain yield on saline
723 soils is improved by an ancestral Na^+ transporter gene. *Nature Biotechnology*, 30, 360-
724 364.
725 Munns R., Rebetzke G.J., Husain S., James R.A. & Hare R.A. (2003). Genetic control of
726 sodium exclusion in durum wheat. *Australian Journal of Agricultural Research*, 54,
727 627-635.
728 Munns R. & Tester M. (2008). Mechanisms of salinity tolerance. *Annual Review of Plant*
729 *Biology*, 59, 651-681.
730 Newman I.A. (2001). Ion transport in roots: measurement of fluxes using ion-selective
731 microelectrodes to characterize transporter function. *Plant Cell and Environment*, 24, 1-
732 14.

733 Pettersen E.F., Goddard T.D., Huang C.C., Couch G.S., Greenblatt D.M., Meng E.C. &
734 Ferrin T.E. (2004). UCSF Chimera - a visualization system for exploratory research and
735 analysis. *Journal of Computational Chemistry*, 25, 1605-1612.
736 Platten J.D., Cotsaftis O., Berthomieu P., Bohnert H., Davenport R.J., Fairbairn D.J., Horie T.,
737 Leigh R.A., Lin H.X., Luan S., Maser P., Pantoja O., Rodriguez-Navarro A.,
738 Schachtman D.P., Schroeder J.I., Sentenac H., Uozumi N., Very A.A., Zhu J.K., Dennis
739 E.S. & Tester M. (2006). Nomenclature for *HKT* transporters, key determinants of plant
740 salinity tolerance. *Trends in Plant Science*, 11, 372-374.
741 Poustini K. & Siosemardeh A. (2004). Ion distribution in wheat cultivars in response to
742 salinity stress. *Field Crops Research*, 85, 125-133.
743 R Core Team (2014). R: a language and environment for statistical computing. R Foundation
744 for statistical computing, Vienna.
745 Rogowsky P.M., Guidet F.L.Y., Langridge P., Shepherd K.W. & Koebner R.M.D. (1991).
746 Isolation and characterization of wheat-rye recombinants involving chromosome arm
747 1ds of wheat. *Theoretical and Applied Genetics*, 82, 537-544.
748 Sali A. & Blundell T.L. (1993). Comparative protein modeling by satisfaction of spatial
749 restraints. *Journal of Molecular Biology*, 234, 779-815.
750 Schymkowitz J.W.H., Rousseau F., Martins I.C., Ferkinghoff-Borg J., Stricher F. & Serrano
751 L. (2005) Prediction of water and metal binding sites and their affinities by using the
752 Fold-X force field. *Proceedings of the National Academy of Sciences of the United*
753 *States of America*, 102, 10147-10152.
754 Shen M.Y. & Sali A. (2006). Statistical potential for assessment and prediction of protein
755 structures. *Protein Science*, 15, 2507-2524.
756 Sippl M.J. (1993). Recognition of errors in three-dimensional structures of proteins. *Proteins-*
757 *Structure Function and Genetics*, 17, 355-362.

758 Suzuki N., Koussevitzky S., Mittler R. & Miller G. (2012). ROS and redox signalling in the
759 response of plants to abiotic stress. *Plant, Cell & Environment*, 35, 259-270.
760 Tester M. & Langridge P. (2010). Breeding technologies to increase crop production in a
761 changing world. *Science*, 327, 818-822.
762 Thoday-Kennedy E.L., Jacobs A.K. & Roy S.J. (2015). The role of the CBL–CIPK calcium
763 signalling network in regulating ion transport in response to abiotic stress. *Plant*
764 *Growth Regulation*, 76, 3-12.
765 Tilbrook J., Schilling R.K., Berger B., Garcia A.F., Trittermann C., Coventry S., Rabie H.,
766 Brien C., Nguyen M. & Tester M. (2017). Variation in shoot tolerance mechanisms not
767 related to ion toxicity in barley. *Functional Plant Biology*, 44, 1194-1206.
768 van Bezouw R.F., Janssen E.M., Ashrafuzzaman M., Ghahramanzadeh R., Kilian B., Graner
769 A., Visser R.G. & van der Linden C.G. (2019). Shoot sodium exclusion in salt stressed
770 barley (*Hordeum vulgare* L.) is determined by allele specific increased expression of
771 *HKT1; 5*. *Journal of Plant Physiology*, 241, 153029.
772 Vieira-Pires R.S., Szollosi A. & Morais-Cabral J.H. (2013). The structure of the KtrAB
773 potassium transporter. *Nature*, 496, 323-328.
774 Waters S., Gilliham M. & Hrmova M. (2013). Plant high-affinity potassium (HKT)
775 transporters involved in salinity tolerance: structural insights to probe differences in ion
776 selectivity. *International Journal of Molecular Sciences*, 14, 7660-7680.
777 Xu B., Waters S., Byrt C.S., Plett D., Tyerman S.D., Tester M., Munns R., Hrmova M. &
778 Gilliham M. (2018). Structural variations in wheat HKT1;5 underpin differences in Na^+
779 transport capacity. *Cellular and Molecular Life Sciences*, 75, 1133-1144.

780
781
782

Figure Legends

Figure 1. Salinity tolerance and 4th leaf Na^+ concentration of Mocho de Espiga Branca relative to 72 bread wheat diversity lines and two Australian cultivars Gladius and Scout in soil with 100 mM NaCl. The 4th leaf Na^+ concentration is determined 11 days after treatment with 100 mM NaCl. Salinity tolerance is defined as projected shoot area (PSA) under 100 mM NaCl relative to 0 mM NaCl determined from the final day of imaging. Data presented as means (n = 3-4 except for Gladius and Scout, where n = 12). The standard error of the mean (SEM) for the 4th leaf Na^+ concentration is presented in Table S1.

Figure 2. Na^+ concentration in the 4th leaf blade, sheath, and roots of Mocho de Espiga Branca, Gladius and Scout in hydroponics. **(a)** Representative image of 6 weeks old plants from the hydroponic experiment with 0, 150 and 200 mM NaCl treatments applied at the emergence of the 4th leaf. M = Mocho de Espiga Branca, G = Gladius and S = Scout. Na^+ concentration in **(b)** 4th leaf blade; **(c)** 4th leaf sheath and **(d)** roots determined 21 days after treatments with 0, 150 and 200 mM NaCl. Data presented as means ± SEM (n = 14). Bars with different letters indicate significant differences determined by two-way ANOVA with Tukey's multiple comparison test at $p \leq 0.05$.

Figure 3. A SNP in Mocho de Espiga Branca *TaHKT1;5-D* results in a L190P amino acid residue variation in the Na^+ transporter TaHKT1;5-D. **(a)** Partial alignment of *TaHKT1;5-D* coding and amino acid sequences in Mocho de Espiga Branca, Gladius and Scout compared to Chinese Spring. **(b)** Schematic of the TaHKT1;5-D protein showing the transmembrane α-helices (TMH 1-9) and selectivity filter α-helices (SFH 1-4) adapted from Xu et al. (2018); the Na^+ selectivity filter motif S78-G233-G353-G457 indicated in blank circles and location of the L190P variant indicated in a grey circle. **(c)** Molecular models of TaHKT1;5-D (left,

yellow) and TaHKT1;5-D L190P (right, salmon) transport proteins in cartoon representations with cylindrical α-helices illustrating 3D folds. Constrictions in selectivity filters are bound by four residues (cpk magenta sticks) that contain Na^+ ions (violet spheres). Black arrows illustrate directional flows of Na^+ that are likely to enter the permeation trajectory by-passing selectivity filter constrictions. Variant residues L190 and L190P (cpk sticks and dots, bold types) between wild-type TaHKT1;5-D and the L190P mutant are indicated; the dots illustrate volumes of van der Waals radii. **(d)** Detailed views of α-helices, which neighbour selectivity filter constriction, containing Na^+ (violet spheres), located near selectivity filter residues S78, G233, G353, G457 (cpk magenta) for TaHKT1;5-D (left) and the L190P mutant (right), which are crucial for permeation function. In each protein, polar contacts (cpk sticks and dots) of L190 (TaHKT1;5-D) and L190P (TaHKT1;5-D L190P) positioned on α-helices 4, are indicated by dashed lines (separations between 2.6 Å and 3.2 Å).

Figure 4. The physiological characterisation of L190P variation in TaHKT1;5-D and the evaluation of the xylem sap Na^+ concentration in Mocho de Espiga Branca. **(a)** Current-voltage (I-V) curve observed from Mocho de Espiga Branca (blue) or Gladius (red) *TaHKT1;5-D* cRNA-injected or H_2O-injected (black) *X. laevis* oocytes exposed to 1 mM Na^+ and 30 mM Na^+ glutamate at a voltage range from -120 to +40 mV. Data represents means ± SEM (n = 3-5). **(b)** Transient co-expression of GFP-TaHKT1;5-D variants with a plasma membrane marker in *N. benthamiana* epidermal cells. Leaves were co-infiltrated with *Agrobacterium tumefaciens* strains harbouring either GFP-TaHKT1;5-D L190 (Gladius) or L190P (Mocho de Espiga Branca) and a plasma membrane marker CBL1n-RFP. GFP signal is shown in green in the left panel while RFP-signal is shown in magenta in the middle panel. Representative images are shown. Scale bars = 10 μm. **(c)** The xylem sap Na^+ concentration of Mocho de Espiga Branca and Gladius under 0 and 150 mM NaCl concentrations. Xylem

833 sap was collected from hydroponically grown plants 21 days after 0 and 150 mM NaCl was
834 applied at the emergence of 4th leaf. Bars with different letters indicate significant differences
835 determined by two-way ANOVA with Tukey's multiple comparison test at $p \leq 0.05$.
836
837 **Figure 5.** Ion fluxes measured at the root elongation zone after removal from 100 mM NaCl.
838 Six to seven days old Mocho de Espiga Branca or Gladius seedlings were treated with 100
839 mM NaCl for two days before removal from the solution, the resultant ion fluxes were
840 measured at the elongation zone (between 200 to 600 µm from the root cap) of the primary
841 root of the plants for 25 min. Net **(a)** Na^+; **(b)** K^+ and **(c)** H^+ fluxes. Cumulative total **(d)** Na^+;
842 **(e)** K^+ and **(f)** H^+ fluxes over 25 min. Data presented as means ± SEM (n = 8-9).
843
844 **Figure 6.** Ion transport model for Mocho de Espiga Branca and Gladius plants under NaCl
845 stress. Colour intensity of the arrows is proportional to the measured ion concentrations, with
846 a greater intensity representing a higher concentration. At the root elongation zone, the
847 direction of the arrow indicates the direction of the ion flux, EP = epidermis, CO = cortex,
848 ED = endodermis, SP = stellar parenchyma and XY = xylem apoplast. TaHKT1;5-D L190P in
849 Mocho de Espiga Branca and TaHKT1;5-D L190 in Gladius are indicated as a white circle.
850 The TaHKT1;5-D L190P variant in Mocho de Espiga Branca leads to reduced retrieval of
851 Na^+ from the xylem into the roots resulting in a greater influx of Na^+ in the xylem sap and a
852 higher accumulation of Na^+ in the leaf blade and sheath compared to Gladius. Mocho de
853 Espiga Branca also has greater Na^+ influx at the root elongation zone compared to Gladius.
854 There was no difference in root Na^+ concentration between the two cultivars. The K^+
855 concentration was also similar between Mocho de Espiga Branca and Gladius both in the
856 roots and xylem sap, however, Mocho de Espiga Branca had less K^+ in the leaf blade and
857 sheath compared to Gladius. In both cultivars, a high concentration of Cl^- was transported in

858 the xylem sap and accumulated to a high concentration in the leaf sheath compared to leaf
859 blade.

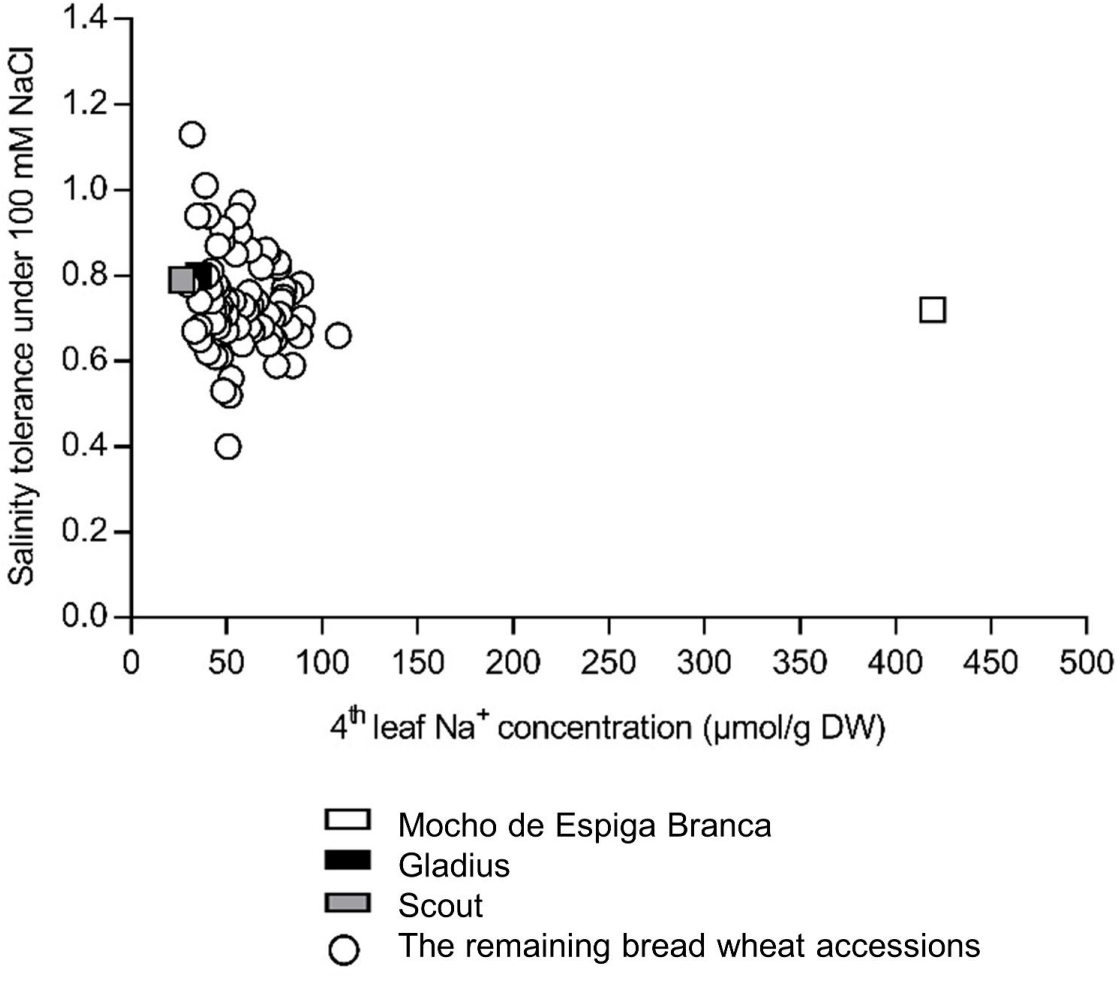
Salinity tolerance under 100 mM NaCl
1.4
1.2
1.0
0.8
0.6
0.4
0.2
0.0
0
50
100
150
200
250
300
350
400
450
500
4th leaf Na+ concentration (µmol/g DW)
Mocho de Espiga Branca
Gladius
Scout
The remaining bread wheat accessions

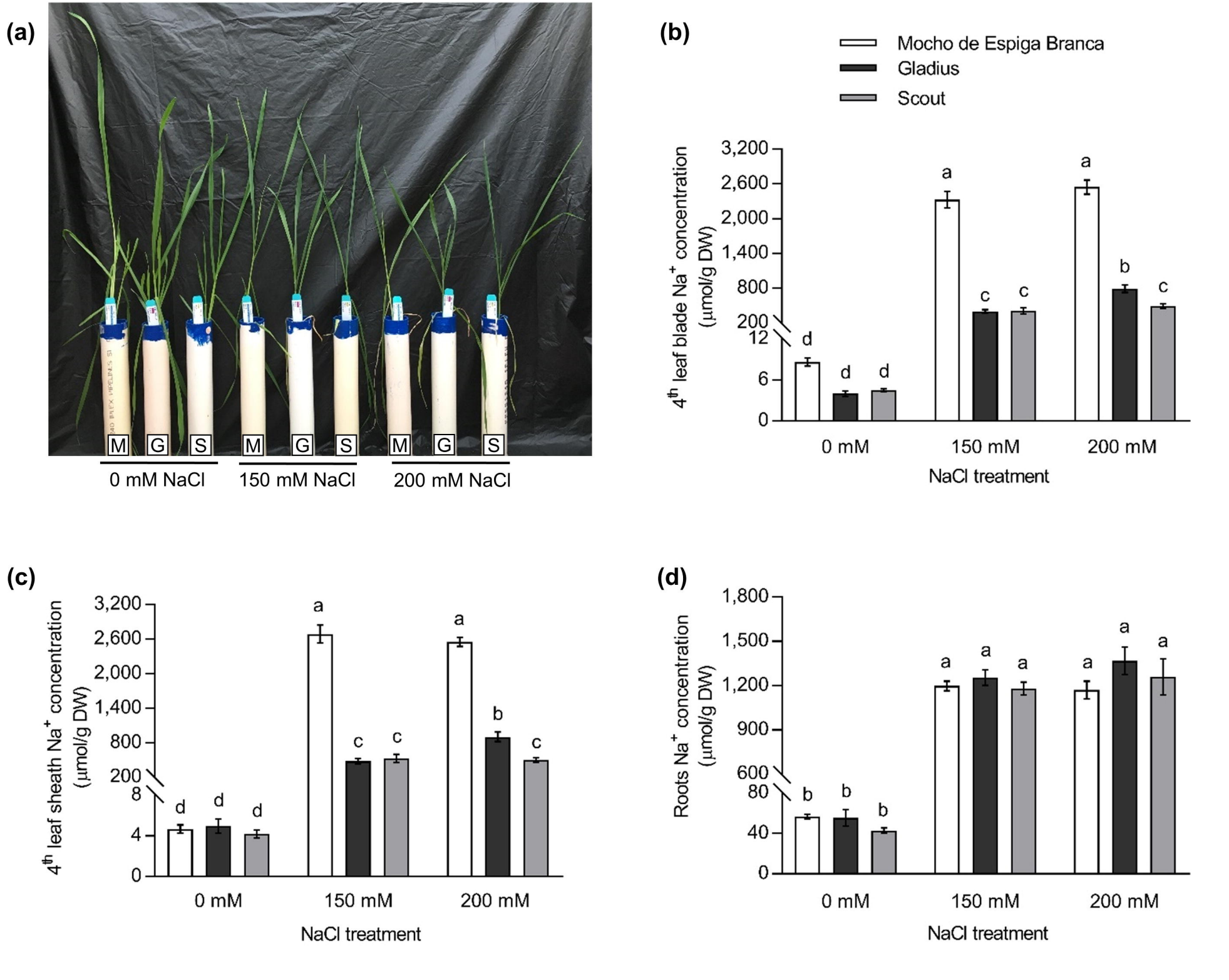
(a)
M
G
S
M
G
S
M
G
S
0 mM NaCl
150 mM NaCl
200 mM NaCl
(b)
Mocho de Espiga Branca
Gladius
Scout
4th leaf blade Na+ concentration (µmol/g DW)
3,200
2,600
2,000
1,400
800
200
12
6
0
d
d
d
a
c
c
a
b
c
0 mM
150 mM
200 mM
NaCl treatment
(c)
4th leaf sheath Na+ concentration (µmol/g DW)
3,200
2,600
2,000
1,400
800
200
8
4
0
d
d
d
a
c
c
a
b
c
0 mM
150 mM
200 mM
NaCl treatment
(d)
Roots Na+ concentration (µmol/g DW)
1,800
1,500
1,200
900
600
80
40
0
b
b
b
a
a
a
a
a
a
0 mM
150 mM
200 mM
NaCl treatment

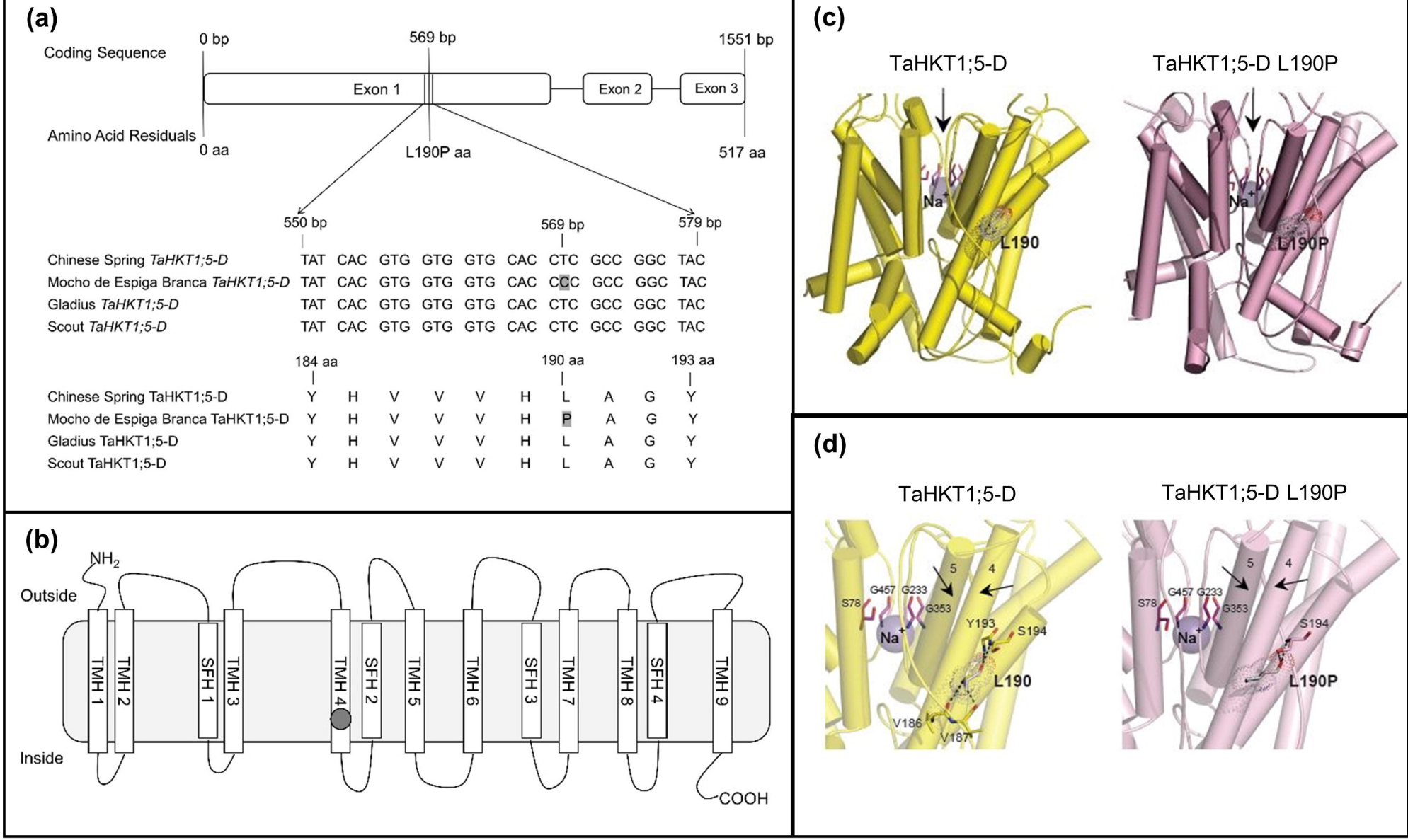
(a)
Coding Sequence
0 bp
569 bp
1551 bp
Exon 1
Exon 2
Exon 3
Amino Acid Residuals
0 aa
L190P aa
517 aa
550 bp
569 bp
579 bp
Chinese Spring TaHKT1;5-D TAT CAC GTG GTG GTG CAC CTC GCC GGC TAC
Mocho de Espiga Branca TaHKT1;5-D TAT CAC GTG GTG GTG CAC CCC GCC GGC TAC
Gladius TaHKT1;5-D TAT CAC GTG GTG GTG CAC CTC GCC GGC TAC
Scout TaHKT1;5-D TAT CAC GTG GTG GTG CAC CTC GCC GGC TAC
184 aa
190 aa
193 aa
Chinese Spring TaHKT1;5-D Y H V V V H L A G Y
Mocho de Espiga Branca TaHKT1;5-D Y H V V V H P A G Y
Gladius TaHKT1;5-D Y H V V V H L A G Y
Scout TaHKT1;5-D Y H V V V H L A G Y
(b)
NH2
Outside
Inside
TMH 1
TMH 2
SFH 1
TMH 3
TMH 4
SFH 2
TMH 5
TMH 6
SFH 3
TMH 7
TMH 8
SFH 4
TMH 9
COOH
(c)
TaHKT1;5-D
TaHKT1;5-D L190P
Na+
L190
L190P
(d)
TaHKT1;5-D
TaHKT1;5-D L190P
5
4
G457
G233
S78
G353
Y193
S194
Na+
L190
L190P
V186
V187

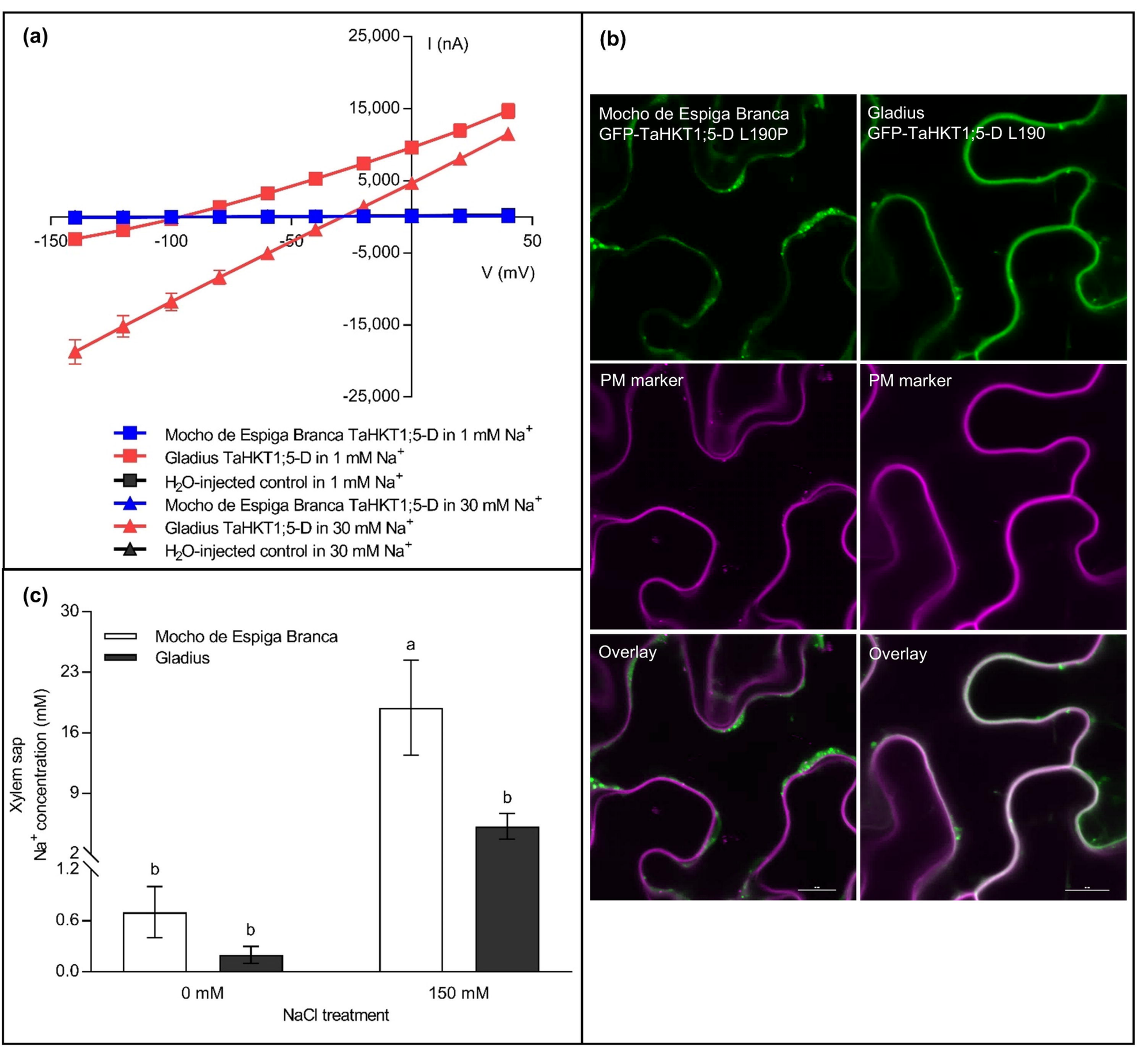
(a)
25,000
15,000
5,000
-5,000
-15,000
-25,000
I (nA)
-150
-100
-50
50
V (mV)
Mocho de Espiga Branca TaHKT1;5-D in 1 mM Na+
Gladius TaHKT1;5-D in 1 mM Na+
H2O-injected control in 1 mM Na+
Mocho de Espiga Branca TaHKT1;5-D in 30 mM Na+
Gladius TaHKT1;5-D in 30 mM Na+
H2O-injected control in 30 mM Na+
(b)
Mocho de Espiga Branca
GFP-TaHKT1;5-D L190P
Gladius
GFP-TaHKT1;5-D L190
PM marker
PM marker
Overlay
Overlay
(c)
Mocho de Espiga Branca
Gladius
Xylem sap
Na+ concentration (mM)
30
23
16
9
2
1.2
0.6
0.0
a
b
b
b
0 mM
150 mM
NaCl treatment

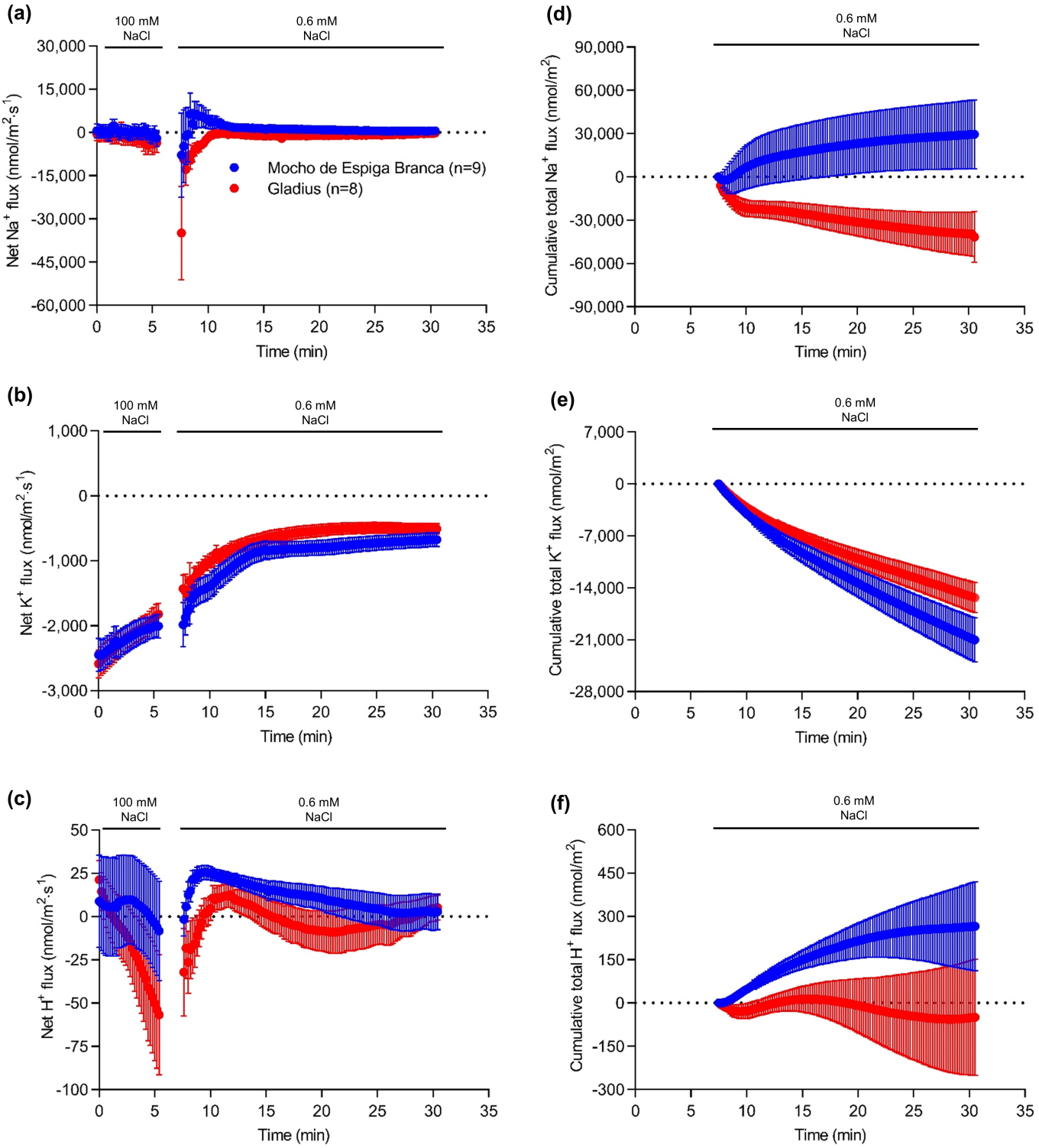

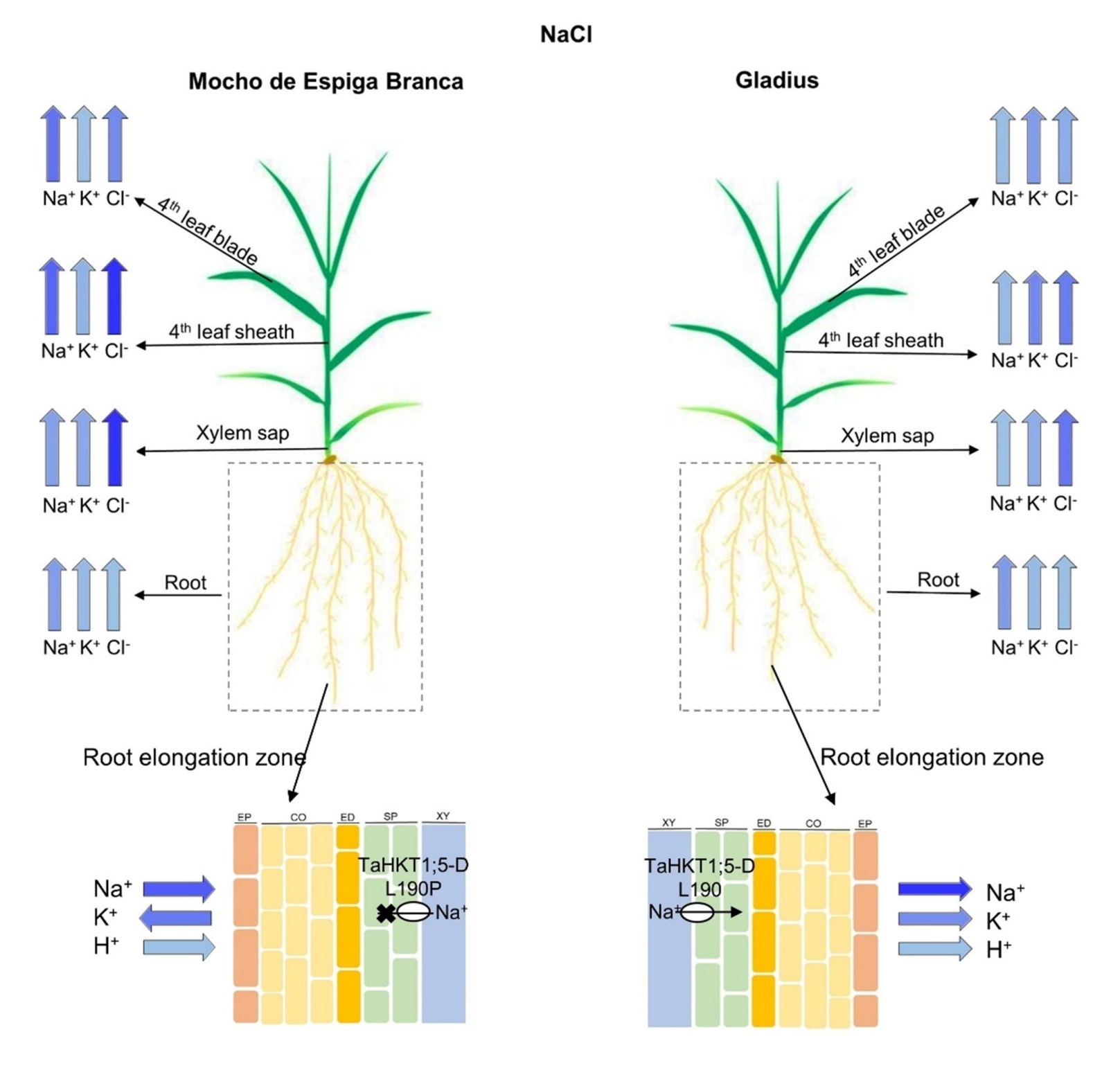
NaCl
Mocho de Espiga Branca
Gladius
Na+ K+ Cl-
4th leaf blade
4th leaf sheath
Xylem sap
Root
Root elongation zone
EP
CO
ED
SP
XY
TaHKT1;5-D
L190P
Na+
K+
H+
TaHKT1;5-D
L190